Biomolecules and Biomedicine
ISSN: 2831-0896 (Print) | ISSN: 2831-090X (Online)
Journal Impact Factor® (2025): 2.8
CiteScore® (2025): 4.7
www.biomolbiomed.com | blog.bjbms.org

The BiomolBiomed publishes an "Advanced Online" manuscript format as a free service to authors in order to expedite the dissemination of scientific findings to the research community as soon as possible after acceptance following peer review and corresponding modification (where appropriate). An "Advanced Online" manuscript is published online prior to copyediting, formatting for publication and author proofreading, but is nonetheless fully citable through its Digital Object Identifier (doi®). Nevertheless, this "Advanced Online" version is NOT the final version of the manuscript. When the final version of this paper is published within a definitive issue of the journal with copyediting, full pagination, etc., the new final version will be accessible through the same doi and this "Advanced Online" version of the paper will disappear.

RESEARCH ARTICLE

Li et al.: HPV-linked macrophage states

HPV-associated macrophage states and expression-based scores in head and neck squamous cell carcinoma

Yanchen Li[#*], Zihui Huang[#] and Anxun Wang

Department of Oral and Maxillofacial Surgery, The First Affiliated Hospital of Sun Yat-sen University, Guangzhou, China

*Correspondence to **Yanchen Li**: liych286@mail2.sysu.edu.cn.

[#]Equally contributed to this work and share first authorship: Yanchen Li and Zihui Huang.

DOI: https://doi.org/10.17305/bb.2026.14972

EARLY ACCESS

ABSTRACT

Human papillomavirus (HPV) status defines contrasting immune ecosystems in head and neck squamous cell carcinoma (HNSCC). We investigated how tumor-associated macrophage (TAM) states and their regulatory programs contribute to this diversity and whether these features can be captured in patient-level expression signatures. We integrated 229,196 single cells from 59 patients with HNSCC (26 HPV-positive and 33 HPV-negative), defined eight TAM states, and combined functional and trajectory analyses with regulon inference, virtual perturbation, and CellChat. A 12-gene Weighted Inflammatory Score (WIS) and a TAM-related score (TRS) were evaluated in independent transcriptomic cohorts. Multiplex immunofluorescence provided representative tissue-level observations. HPV-positive tumors showed a lymphoid-enriched landscape, whereas HPV-negative tumors had greater TAM and fibroblast representation. Patient-level comparisons identified lower Inflammatory TAM and Pro-tumor/Secretory TAM fractions in HPV-positive patients (Benjamini–Hochberg [BH]-adjusted p = 0.0172 and 0.0486, respectively). Regulon analysis and virtual SNAI1 perturbation converged on inflammatory, leukocyte migration, and chemotaxis programs. Targeted CellChat analysis identified a candidate epithelial-source HLA-DRA–CD4 interaction involving seven TAM recipient states in HPV-positive tumors compared with two in HPV-negative tumors. Fixed-coefficient WIS achieved an area under the receiver operating characteristic curve (AUC) of 0.938 (95% confidence interval [CI] 0.863–1.000) across 36 independent patients. TRS provided complementary HPV-status discrimination, with a cross-validated AUC of 0.783 in The Cancer Genome Atlas (TCGA) and an external AUC of 0.649 in GSE40774. HPV-associated immune differences in HNSCC involve distinct macrophage states, candidate SNAI1-linked inflammatory and migratory regulatory programs, and inferred epithelial–TAM communication patterns. WIS and TRS connect selected single-cell observations with patient-level transcriptomic features and may guide future mechanistic and validation studies.

Keywords: Human papillomavirus, head and neck squamous cell carcinoma, tumor-associated macrophages, SNAI1, inflammatory signature, single-cell RNA sequencing.

EARLY ACCESS

INTRODUCTION

Head and neck squamous cell carcinoma (HNSCC) comprises a heterogeneous group of malignancies arising from the mucosal epithelium of the oral cavity, oropharynx, hypopharynx, and larynx. Despite sharing the same histological classification, HNSCC tumors exhibit substantial heterogeneity in their etiology, biological characteristics, and clinical outcomes [1–4]. Treatment is tailored to the anatomical site, disease stage, resectability, functional preservation and patient condition. Early-stage HNSCC is commonly managed with surgery or definitive radiotherapy, whereas locally advanced disease often requires multimodal treatment, including surgery followed by risk-adapted radiotherapy or chemoradiotherapy, or definitive cisplatin-based concurrent chemoradiotherapy. For recurrent or metastatic disease, systemic options include platinum-based chemotherapy, epidermal growth factor receptor (EGFR)-targeted treatment with cetuximab, and programmed cell death protein 1 (PD-1) immune checkpoint inhibitors [1]. Neoadjuvant and perioperative strategies are also being investigated or incorporated in selected clinical settings [5,6].

Despite advances in management, therapeutic responses and prognosis differ markedly among patients with HNSCC. Notably, HPV-positive oropharyngeal HNSCC generally responds more favorably to treatment and is associated with better survival than HPV-negative disease [2,4]. These clinical differences coincide with distinct tumor immune microenvironments. Tumor-associated macrophages (TAMs), which participate in inflammation, antigen-presentation-associated processes, tissue remodeling and immune regulation, are important components of these ecosystems [7,8]. Previous studies have reported greater infiltration of activated T cells, B cells and organized lymphoid structures in HPV-positive tumors, whereas HPV-negative tumors more frequently display prominent macrophage- and stroma-associated features [9–11]. Such observations point to differences in both immune-cell composition and functional state across HPV-defined disease groups.

Single-cell and spatial transcriptomic studies have further resolved heterogeneous TAM populations in HNSCC, including SPP1-associated, inflammatory and interferon-responsive phenotypes, and have described HPV-associated differences in macrophage organization and function [12–16]. Recent work has also highlighted tumor-cell interferon and major histocompatibility complex class II (MHC-II)

EARLY ACCESS

programs, together with spatially organized tumor–immune interactions [17–19]. Nevertheless, it remains incompletely understood how HPV-associated TAM states relate to candidate transcriptional regulators and epithelial–macrophage communication networks. In particular, the programs linked to inflammatory and migratory TAM functions, and whether their transcriptional features can be evaluated at the patient level, warrant closer investigation.

To address these questions, we integrated single-cell RNA-sequencing profiles from 59 patients with HNSCC (229,196 cells) to characterize eight TAM states and their HPV-associated compositional and functional differences. We combined trajectory inference, cell–cell communication analysis, regulon inference and computational virtual perturbation to explore candidate regulatory networks, with particular attention to SNAI1-linked inflammatory and migratory programs. We also evaluated a 12-gene Weighted Inflammatory Score (WIS) and a complementary TAM-related score (TRS) in patient-level transcriptomic cohorts, alongside representative multiplex tissue staining. By relating TAM-state heterogeneity to candidate regulatory programs and patient-level expression patterns, this study offers a focused view of HPV-associated immune remodeling and provides testable hypotheses for future mechanistic and clinical validation.

MATERIALS AND METHODS

Single-cell cohorts, quality control and integration

We analyzed the public HNSCC single-cell datasets GSE234933 (23 patients: 8 HPV-positive, 15 HPV-negative), GSE181919 (20: 7 positive, 13 negative) and GSE182227 (16: 11 positive, 5 negative), comprising 59 patients and 229,196 quality-controlled cells. Patient and sample identifiers, HPV status and available clinical information were reconciled with the source publications, supplementary tables and GEO annotations (Supplementary Table S1). Patient-level histories were distinguished from specimen annotations.

Quality control was performed with Seurat v5, retaining cells with 500–8,000 detected genes and mitochondrial RNA below 20% in GSE234933/GSE182227 or 10% in GSE181919. Integration followed LogNormalize, selection of 2,000 highly variable genes, principal component analysis (PCA), Harmony correction in PCA space, clustering and UMAP visualization [20–22]. Ten major lineages—tumor

EARLY ACCESS

epithelium, cancer-associated fibroblasts (CAFs), vascular endothelial cells, lymphatic endothelial cells, TAMs, T/NK cells, B cells, plasma cells, plasmacytoid dendritic cells and mast cells—were annotated using canonical markers. Quality-control and integrated-cell maps are shown in Supplementary Figure S1.

TAM subclustering and patient-aware cell composition

Myeloid cells were extracted, and cells expressing markers of other lineages (including CD3D, immunoglobulin genes or COL1A1) were excluded. Cell-cycle S/G2M scores and percent.ribo were regressed out, and cell-cycle- and ribosome-associated genes were excluded from variable features before subclustering at resolution 0.3. TAM states were annotated using lineage and functional markers. Patient-level TAM-state comparisons were restricted to GSE234933 because the other cohorts contained too few annotated TAMs for reliable state-proportion analysis.

The proportions of 10 major cell lineages were calculated for each of the 59 patients. Associations between cell composition and HPV status were assessed using binomial least absolute shrinkage and selection operator (LASSO) regression implemented in glmnet ($\alpha = 1$), with standardized predictors and an intercept. Five-fold cross-validation stratified by HPV status was performed to select the optimal penalty parameter based on binomial deviance. Model discrimination and predictive performance were further assessed using nested five-fold cross-validation, with patient-level out-of-fold predictions used to calculate the area under the receiver operating characteristic curve (AUC), Brier score, log loss, and DeLong 95% confidence intervals.

Within GSE234933 (8 HPV-positive and 15 HPV-negative patients), patient-level fractions of the eight TAM states were compared by two-sided Mann–Whitney U tests, with Benjamini–Hochberg (BH) adjustment. A separate patient-level regression estimated the HPV-group contrast in Inflammatory TAM fraction; a sensitivity model additionally adjusted for ever-smoking status. Comparisons and clinical sensitivity analyses used patients, not cells, as independent observations.

Weighted Inflammatory Score construction and evaluation

The weighted inflammatory score (WIS) was constructed using GSE234933. The top 50 differentially expressed genes were selected as candidates for LASSO-based

EARLY ACCESS

feature selection. Gene weights were subsequently estimated by binomial logistic regression using normalized expression values from the Seurat RNA data layer. HPV status was assigned at the patient level, whereas coefficients were estimated using individual cells. WIS was calculated as the weighted sum of the selected gene expression values, excluding the fitted intercept. The gene list and complete scoring coefficients are provided in Supplementary Table S3.

The fixed WIS coefficients were applied to GSE181919 and GSE182227 without model refitting. Cell-level WIS values were averaged for each patient, and discrimination of HPV status was evaluated using receiver operating characteristic (ROC) analysis and DeLong 95% confidence intervals. As a sensitivity analysis within the GSE234933 development cohort, the fixed score was also averaged per patient across all cells or restricted to 8,844 TAMs (n=23), without coefficient refitting. Separately, single-sample gene set enrichment analysis (ssGSEA) was performed using the same genes, followed by logistic regression within the TCGA-HNSC cohort.

Trajectory inference and functional-state scoring

Monocle3 was used to infer branched TAM transcriptional trajectories and pseudotime [23–24]. Trajectory orientation was informed by the higher-developmental-potential region defined with CytoTRACE2 applied to raw counts [25]; prior root-selection sensitivity analysis was incorporated into the interpretation. HPV-stratified pseudotime and CytoTRACE2 distributions were presented descriptively. Functional programs—including glycolysis, oxidative phosphorylation and antigen processing/presentation—were scored using curated MSigDB/KEGG gene sets and Seurat module scores [26–27].

CellChat inference of epithelial–TAM communication

Cell–cell communication between tumor epithelial cells and eight TAM states was investigated using CellChat (v2.2.0.9001) in GSE234933 [28]. Separate communication networks were constructed for HPV-positive and HPV-negative samples using normalized RNA expression data and CellChatDB.human. Overexpressed signaling genes and interactions were identified, followed by protein–protein interaction network smoothing using PPI.human. Communication probabilities were inferred using computeCommunProb(type = "triMean", raw.use =

EARLY ACCESS

FALSE), with interactions filtered using filterCommunication(min.cells = 10) and subsequently aggregated at the signaling pathway level. Directed epithelial-to-TAM interactions involving MHC-II and MIF signaling were extracted using subsetCommunication for comparison between HPV groups.

Regulon inference and virtual transcription-factor perturbation

Candidate gene-regulatory networks were inferred using a custom xgboost.XGBRegressor framework. Each target gene was modeled using candidate transcription-factor expression (n_estimators=200; learning_rate=0.05; max_depth=4; subsample=0.8; colsample_bytree=0.8). The colsample_bytree setting introduced feature subsampling during tree construction, potentially reducing dependence on individual transcription-factor predictors. Gain-based feature importance was used to define candidate regulatory edges, followed by pySCENIC motif pruning and AUCell scoring [29–30]. Regulon activity was compared across TAM states; TCF4 refers to TCF4/E2-2, not TCF7L2.

scTenifoldKnk [31] was used to simulate SNAI1 perturbation in 971 Inflammatory TAMs (1,611 retained genes) and TCF4 perturbation in 723 Stress/ISG TAMs (1,541 genes). Expressed genes were selected from the 2,000 most variable features plus the target gene. Predicted differential-regulation statistics were examined by GO Biological Process enrichment and gene-set enrichment analysis [26–27,32], with BH correction where reported in the supplied outputs.

TAM-related score, frozen external testing and survival association

Stress/ISG-TAM and Inflammatory-TAM gene signatures used the first 50 ordered markers of each original state-specific list, restricted to the 10,026-gene universe observed in both TCGA-HNSC and GSE40774, leaving 41 Stress and 37 Inflammatory genes. ssGSEA scores were calculated with GSVA 2.0.7 and normalize=FALSE. One TCGA primary-tumor sample per patient was retained, and interpretable HPV status was assigned preferentially by in situ hybridization with p16 used when ISH was missing. A binomial logistic model was trained in 121 HPV-annotated TCGA patients (39 positive, 82 negative). Signature means/SDs, intercept and regression coefficients were fixed before applying predictions to independent GSE40774 patients (n=134; 58 positive, 76 negative).

EARLY ACCESS

The model was TRS = 0.927826 x Stress_Z - 1.505119 x Inflam_Z and logit{Pr(HPV-positive)} = -1.045709 + TRS. Stress_Z = (Stress_ssGSEA - 1567.463)/828.980, and Inflam_Z = (Inflam_ssGSEA - 2526.084)/511.944; both center and scale values came exclusively from TCGA. Discrimination was summarized by apparent TCGA ROC AUC, fivefold patient-level out-of-fold TCGA AUC and frozen-coefficient GSE40774 ROC AUC with descriptive DeLong intervals. External calibration intercept, slope and Brier score were recorded (Supplementary Table S4).

Survival analyses examined the separate TAM-state signatures rather than the TRS classifier. Kaplan–Meier high/low groups were defined by the median score across 517 survival-eligible TCGA primary tumors; the same cutoffs were used within HPV strata, and six log-rank tests underwent BH correction. Cox hazard ratios (HRs) per one-standard-deviation increase were estimated without and with age/sex/stage adjustment (BH correction across four coefficient tests). Two age/sex-adjusted HPV-by-signature interactions in 120 HPV-annotated cases were also BH-adjusted. Denominators and event counts are provided in Supplementary Table S5.

Multiplex immunofluorescence

Formalin-fixed, paraffin-embedded HNSCC sections from ten patients (five HPV-positive and five HPV-negative) were assessed by multiplex immunofluorescence. Sections were stained for HLA-DR (1:1000; clone 10-D8-R, HUABIO), CD68 (1:2000; ab955, Abcam) and CD163 (1:2000; clone JA51-30, HUABIO), with DAPI nuclear counterstaining. Images were acquired on a TissueFAXS platform (TissueGnostics, Vienna, Austria) using a 20× objective. Representative fields were selected according to tissue integrity, focus and absence of obvious folds or necrosis.

Ethical statement

The ethical, medical and scientific aspects of the research were reviewed and approved by the Ethics Committee of the First Affiliated Hospital, Sun Yat-Sen University before study initiation (approval no. [2022]474).

The requirement for informed consent was waived by the Ethics Committee of the First Affiliated Hospital of Sun Yat-sen University because this study retrospectively used archived, de-identified tissue specimens.

EARLY ACCESS

Statistical analysis

All statistical tests were two-sided unless otherwise specified, and multiple-testing correction was applied where indicated. Missing clinical covariates were not imputed.

RESULTS

HPV status delineates lymphoid-rich and macrophage/stroma-rich HNSCC ecosystems

Among 229,196 cells from 59 patients (26 HPV-positive, 33 HPV-negative), 22 clusters representing ten major lineages were identified (Figure 1A–C; Supplementary Figure S1). Pooled B-cell and plasma-cell proportions were higher in HPV-positive tumors (10.5% versus 4.5%; 4.0% versus 3.3%), whereas TAM and CAF proportions were higher in HPV-negative tumors (13.0% versus 7.6%; 10.0% versus 5.6%; Figure 1D). Clinical-source review recovered age, sex and smoking history for 39 patients, primary tumor anatomical site for 59, alcohol-use history for 16 and patient-level clinical T/N-stage annotations for 36 (Supplementary Table S1).

The patient-level LASSO selected B cells (+3.743), lymphatic endothelial cells (+0.740), TAMs (−5.502) and CAFs (−0.789) at lambda.min=0.07166 (Figure 1E); only B cells and TAMs remained at lambda.1se. Nested patient-level cross-validation yielded an out-of-fold AUC of 0.724 (approximate 95% CI 0.594–0.854), Brier score 0.208 and log loss 0.612. This supports the lymphoid-versus-macrophage composition contrast at the patient level.

Eight macrophage states reveal HPV-associated inflammatory and secretory diversity

Eight TAM states were identified: Tissue-Resident, APOE+, SPP1+, Monocyte-like, Inflammatory, Stress/ISG, Pro-tumor/Secretory, and ISG-activated (Figure 2A–C). Of 8,922 annotated TAMs, 8,844 were derived from GSE234933, supporting patient-level state-composition analyses in the 23 patients from this cohort. The overall TAM-state composition differed between HPV-positive and HPV-negative tumors (Figure 2D). At the patient level, HPV-positive patients had lower Inflammatory TAM fractions (median 0.015 versus 0.089; Mann–Whitney p=0.0021, BH-FDR=0.0172) and Pro-tumor/Secretory TAM fractions (median 0.000 versus 0.020; p=0.0122, BH-FDR=0.0486; Supplementary Table S2). A separate patient-level

EARLY ACCESS

regression estimated an Inflammatory TAM difference of −0.1367 (95% CI −0.2635 to −0.0100; p=0.0357; n=23). Adjustment for ever-smoking attenuated the difference (−0.0951; 95% CI −0.2283 to 0.0381; p=0.1520; Supplementary Table S2), while limited overlap in tumor site between HPV groups precluded stable site adjustment. Figure 2E reports nominal significance from an earlier exploratory model, whereas Supplementary Table S2 provides final BH-adjusted patient-level comparisons and separate regression/smoking analyses. These distinct analyses explain the differing significance patterns; the patient-level findings remain the primary evidence for HPV-associated TAM-state differences.

A 12-gene inflammatory signature captures HPV-associated biology across independent cohorts

A 12-gene signature comprising CCL20, INHBA, CLEC5A, EREG, CXCL1, MCEMP1, CD300E, THBD, OSM, TNF, PHLDA1 and AQP9 was selected for WIS analysis (Figure 2F–H; Supplementary Table S3). Within GSE234933, patient-aggregated sensitivity analyses using the fixed score yielded AUCs of 0.975 (95% CI 0.921–1.000) across all cells and 0.992 (0.969–1.000) within 8,844 TAMs (n=23). With weights fixed from GSE234933, patient-level AUCs were 0.934 (95% CI 0.816–1.000; n=20) in GSE181919 and 0.873 (0.650–1.000; n=16) in GSE182227. Figure 2G shows the pooled validation cohort's WIS distribution by HPV status; the combined AUC was 0.938 (0.863–1.000; n=36; Figure 2H). These fixed-coefficient external results establish HPV-status discrimination, rather than independent confirmation of macrophage-specific functional activity. A separately fitted TCGA-HNSC ssGSEA classifier using the same genes had a cohort-internal AUC of 0.813 (Figure 2I), not an independent validation of the fixed WIS.

Exploratory TCGA gene-level Cox estimates for PHLDA1 and EREG (Figure 2J) suggested possible links between inflammatory transcriptional features and clinical outcome. The EREG p value of approximately 0.045 was nominal, and the observed association in bulk tumor tissue cannot be attributed exclusively to macrophages.

Trajectory and metabolic analyses link macrophage-state diversity to functional organization

Monocle3 positioned the eight TAM states along a branched transcriptional continuum (Figure 3A–C). CytoTRACE2 suggested higher developmental-potential

EARLY ACCESS

scores in Monocyte-like and SPP1+ cells and lower scores in Stress/ISG and ISG-activated cells (Figure 3D–F). Pathway scoring highlighted HPV-associated differences in glycolysis, pyruvate metabolism, antigen processing/presentation and inflammatory programs (Figure 3G).

Epithelial–TAM communication reveals HPV-associated MHC-II and MIF network patterns

CellChat identified different epithelial–TAM communication patterns by HPV status (Figure 4A–C). GSE234933 yielded 7,886 inferred interactions (aggregate weight 47.81) in HPV-positive tumors and 11,740 (weight 65.85) in HPV-negative tumors. In the full network, MHC-II pathway probability was 29.753 versus 30.880, and the HPV-positive-minus-negative MIF pathway difference was −0.261 (Figure 4D). Whole-network patterns were considered separately from targeted epithelial-source links.

The epithelial-source HLA-DRA–CD4 candidate entry connected seven TAM recipient states in HPV-positive tumors and two in HPV-negative tumors (Figure 4E), representing state-specific links for the same annotated molecular entry. MIF-related epithelial-to-TAM connections occurred in both groups (21 versus 24), including MIF–(CD74+CD44), MIF–(CD74+CXCR4) and MIF–(CD74+CXCR2) (Figure 4F). Figure 4G and the 54 records in Supplementary Table S6 provide expression and interaction details.

A SNAI1-linked inflammatory and migratory program emerges from TAM regulatory networks

Inflammatory TAMs showed higher SNAI1- and MECP2-associated regulon activity than Monocyte-like cells (Figure 5A,F). Virtual SNAI1 knockout with scTenifoldKnk predicted regulatory shifts involving SNAI1, FCN1 and APOBEC3A (Figure 5G). GO enrichment highlighted leukocyte and myeloid-cell migration, chemotaxis and macrophage migration (Figure 5H), while GSEA implicated immune-response programs (Figure 5I). Although these analyses do not establish direct regulatory relationships or causality, the convergent findings collectively suggest the presence of a SNAI1-associated inflammatory and migratory regulatory network in this TAM state.

EARLY ACCESS

Stress/ISG TAMs showed increased TCF4-, HESX1- and TFE3-associated regulon activity relative to Monocyte-like cells (Figure 5B). Virtual TCF4 knockout predicted changes involving APOE, PLD3, LGMN and APOC1 (Figure 5C), with enrichment for T-cell activation, leukocyte adhesion, chemotaxis and antigen processing/presentation (Figure 5D–E). These results suggest complementary TCF4-associated stress/interferon and SNAI1-associated inflammatory/migratory programs across TAM states.

TAM-state signatures extend single-cell discoveries to patient-level observations

In 517 TCGA primary tumors with survival data (220 deaths), Kaplan–Meier comparisons for Stress/ISG-TAM and Inflammatory-TAM signatures were nonsignificant overall (p=0.208 and p=0.405; Figure 6A–D). An HPV-negative subgroup association was nominal for Inflammatory TAMs (n=81, 26 deaths; p=0.045), but the six-test BH-FDR was 0.272. Age/sex/stage-adjusted Cox HRs were 1.13 (95% CI 0.97–1.31; p=0.106) for Inflammatory TAMs and 0.94 (0.83–1.08; p=0.390) for Stress/ISG TAMs. An exploratory HPV-by-Inflammatory-TAM interaction yielded HR=0.25 (p=0.019; BH-FDR=0.038), warranting cautious interpretation in the small HPV-annotated survival subset.

We next combined standardized Stress/ISG and Inflammatory signatures into the TAM-related score (TRS). In TCGA (n=121; 39 HPV-positive, 82 HPV-negative), coefficients were +0.927826 and −1.505119, respectively (intercept −1.045709). TRS had an apparent AUC of 0.800 (95% CI 0.715–0.885) and fivefold patient-level out-of-fold AUC of 0.783 (0.694–0.872). External application of fixed coefficients and TCGA standardization to GSE40774 (n=134; 58 HPV-positive, 76 HPV-negative) yielded an AUC of 0.649 (95% CI 0.557–0.741) and a Brier score of 0.240. The calibration-in-the-large intercept was 0.089, while the fitted logistic recalibration curve had an intercept of −0.057 and a slope of 0.520 (Figure 6H-I; Supplementary Table S4). These findings are not yet sufficient to establish its utility for clinical risk stratification, but they support its value as an HPV-associated expression measure.

Multiplex tissue staining provides a histological perspective on macrophage programs

Multiplex immunofluorescence was examined in tissues from five HPV-positive and five HPV-negative patients (Figure 7). In the selected HPV-negative representative

EARLY ACCESS

field, CD68 and CD163 staining was more conspicuous, whereas the selected HPV-positive field displayed more prominent HLA-DR-associated staining. Although the multiplex staining was evaluated qualitatively, these representative tissue-level observations were consistent with the macrophage enrichment and antigen presentation-related transcriptional patterns identified by single-cell analysis, providing complementary tissue-level support for these findings.

DISCUSSION

This study adds a state-resolved view of TAM biology to previous descriptions of HPV-associated HNSCC immune ecosystems. Across 59 patients and 229,196 cells, we identified eight TAM states and examined their HPV-associated distribution, functional features, inferred epithelial–immune communication and regulatory programs. Beyond the already recognized lymphoid-versus-stromal contrasts [9–14], a particular contribution is the SNAI1-associated inflammatory/migratory signature considered alongside complementary TCF4-related features and patient-level expression scores. These observations refine the questions that can be tested in subsequent functional and larger clinical studies.

One finding of interest is the SNAI1-associated program in Inflammatory TAMs. SNAI1 is best known for malignant-cell epithelial–mesenchymal transition, and tumor-cell Snail has previously been linked to cytokine secretion and macrophage recruitment [33–34]. Our regulon and virtual-perturbation results implicate leukocyte migration, macrophage chemotaxis and related inflammatory responses, suggesting a candidate role for SNAI1-linked networks in macrophage functional identity. These associations do not establish direct SNAI1-dependent regulation and require targeted experimental confirmation. The distinct TCF4-associated program in Stress/ISG TAMs points to another candidate axis involving interferon responsiveness, antigen presentation and immune interactions.

Our state-resolved results also put previously described macrophage populations into a broader HPV-associated context. The SPP1+ state corresponds to a recognized macrophage transcriptional phenotype implicated in tumor remodeling [15], whereas the Stress/ISG and ISG-activated states display features related to interferon-responsive macrophages. Prior analysis of HNSCC identified CXCL9-versus-SPP1 macrophage polarity as a spatially organized axis linked to the broader immune

EARLY ACCESS

context [35]; separately, a study of HNSCC lymph-node metastasis characterized TREM2+ TAMs associated with exhausted CD8+ T cells and an SPP1-related communication program [36]. These published CXCL9+ and TREM2+ programs are informative comparators, but neither should be assumed to map one-to-one onto our eight transcriptional clusters across different datasets and annotation systems. The principal additional insight of our atlas is therefore the SNAI1-associated inflammatory/migratory regulon and complementary TCF4-related state organization, rather than merely assigning another TAM subtype name.

A second important finding concerns the organization of epithelial–macrophage communication. CellChat identified the database-annotated HLA-DRA–CD4 entry as a candidate epithelial-source MHC-II interaction spanning a broader range of TAM recipient states in HPV-positive tumors, alongside MIF-associated connections detected in both HPV groups. The distinction between recipient-state coverage and whole-network pathway weight is biologically informative: a pathway may have different overall inferred probabilities while involving different cellular partners. This state-specific view complements reports of B-cell-rich niches, tertiary lymphoid structures and CXCL13-producing T-cell-associated lymphoid organization in HPV-positive HNSCC [10,12–14], as well as recent observations of malignant-cell interferon/MHC-II programs [17–19]. It therefore provides an additional framework for examining how antigen-presentation-related epithelial transcripts and innate immune populations are organized within HPV-defined tumors.

Patient-level expression signatures provide complementary perspectives on TAM-associated biology. WIS captures an inflammatory transcriptional pattern that distinguished HPV status in two independent patient cohorts, suggesting that selected features identified through single-cell analysis can be detected at the patient level. Patient-aggregated sensitivity analyses, including the TAM-restricted evaluation, retained this HPV-associated expression signal, complementing the independent fixed-coefficient results. In contrast, TRS integrates Stress/ISG-TAM and Inflammatory-TAM signatures to reflect broader differences in macrophage-associated functional programs, although its more modest external performance indicates limited generalizability. Further independent validation is required to establish whether WIS and TRS can serve as reliable indicators of macrophage abundance, prognosis, or clinical risk before their clinical application. Nevertheless,

EARLY ACCESS

these two scores offer complementary expression-based approaches to investigating HPV-associated immune heterogeneity, providing a framework for linking macrophage-related transcriptional programs with patient-level molecular profiles.

Limitations

Several limitations warrant consideration. Strong HPV–tumor-site alignment restricted confounder adjustment, particularly in the 23-patient TAM cohort; prior treatment and recurrence histories were incompletely documented in GSE182227. Although cell-level estimation of WIS coefficients can introduce within-patient dependence, patient-aggregated sensitivity analyses and fixed-coefficient validation in independent cohorts both retained HPV-status discrimination. Retained proportional-hazards diagnostics were also unavailable, and nominal survival associations need replication. Trajectories, CellChat and virtual perturbations remain inferential, while multiplex staining was qualitative. Although these findings are not yet ready for clinical application, this exploratory study provides testable hypotheses and an analytical framework for future mechanistic investigations and prospective clinical validation.

CONCLUSION

In conclusion, HPV-associated HNSCC immune differences include variation in TAM composition, functional states and candidate regulatory networks. A SNAI1-linked inflammatory/migratory pattern, complementary TCF4-associated stress/interferon features and inferred epithelial-to-TAM MHC-II/MIF interactions provide a more detailed view of macrophage heterogeneity. WIS and TRS extend selected observations to patient-level expression measures. These findings offer hypotheses and a framework for further experimental and clinical validation.

Conflicts of interest: Authors declare no conflicts of interest.

Funding: This work was supported by funding from the National Natural Science Foundation of China (No. 82372868, 82173041).

Data availability: The primary single-cell datasets are publicly available from GEO (GSE234933, GSE181919 and GSE182227); auxiliary immune analyses also drew on GSE164690. The external HPV-status validation dataset is GSE40774, and TCGA-HNSC data are available through The Cancer Genome Atlas. Derived patient-level

EARLY ACCESS

source and model summary tables, including the complete clinical metadata with explicit missing values, are supplied in Supplementary Tables S1–S6.

Analysis code availability: Representative analysis scripts, including the patient-level composition LASSO, WIS model, CellChat inspection, SCENIC code, and scTenifoldKnk analysis, are supplied as Supplementary Code. Original source data remain accessible via their public repositories. Additional implementation files may be requested from the corresponding author.

Submitted: September 2, 2026
Accepted: November 5, 2026
Published online: November 19, 2026

EARLY ACCESS

REFERENCES

1. Johnson DE, Burtness B, Leemans CR, Lui VWY, Bauman JE, Grandis JR. Head and neck squamous cell carcinoma. Nat Rev Dis Primers. 2020;6(1):92. https://doi.org/10.1038/s41572-020-00224-3

2. Ang KK, Harris J, Wheeler R, Weber R, Rosenthal DI, Nguyen-Tân PF, et al. Human papillomavirus and survival of patients with oropharyngeal cancer. N Engl J Med. 2010;363(1):24–35. https://doi.org/10.1056/NEJMoa0912217

3. The Cancer Genome Atlas Network. Comprehensive genomic characterization of head and neck squamous cell carcinomas. Nature. 2015;517(7536):576–82. https://doi.org/10.1038/nature14129

4. Gameiro SF, Evans AM, Mymryk JS. The tumor immune microenvironments of HPV+ and HPV− head and neck cancers. WIREs Mech Dis. 2022;14(2):e1539. https://doi.org/10.1002/wsbm.1539

5. He Q, Huang S, Tang D, Cao C, Zhou W, Ling R, et al. Neoadjuvant chemotherapy plus anlotinib in the treatment of resectable head and neck squamous cell carcinoma: A pilot phase II trial. Cancer Commun (Lond). 2025;45(5):632–6. https://doi.org/10.1002/cac2.70006

6. Guo SB, Hu LS, Huang WJ, Zhou ZZ, Luo HY, Tian XP. Comparative investigation of neoadjuvant immunotherapy versus adjuvant immunotherapy in perioperative patients with cancer: a global-scale, cross-sectional, and large-sample informatics study. Int J Surg. 2024;110(8):4660–71. https://doi.org/10.1097/JS9.0000000000001479

7. Mantovani A, Allavena P, Marchesi F, Garlanda C. Macrophages as tools and targets in cancer therapy. Nat Rev Drug Discov. 2022;21(11):799–820. https://doi.org/10.1038/s41573-022-00520-5

8. Bisheshar SK, van der Kamp MF, de Ruiter EJ, Ruiter LN, van der Vegt B, Breimer GE, et al. The prognostic role of tumor associated macrophages in squamous cell carcinoma of the head and neck: a systematic review and meta-analysis. Oral Oncol. 2022;135:106227. https://doi.org/10.1016/j.oraloncology.2022.106227

EARLY ACCESS

9. Qureshi HA, Zhu X, Yang GH, Steadele M, Pierce RH, Futran ND, et al. Impact of HPV status on immune responses in head and neck squamous cell carcinoma. Oral Oncol. 2022;127:105774. https://doi.org/10.1016/j.oraloncology.2022.105774

10. Zhang S, Wang B, Ma F, Tong F, Yan B, Liu T, et al. Characteristics of B lymphocyte infiltration in HPV+ head and neck squamous cell carcinoma. Cancer Sci. 2021;112(4):1402–16. https://doi.org/10.1111/cas.14834

11. Tosi A, Parisatto B, Menegaldo A, Spinato G, Guido M, Del Mistro A, et al. The immune microenvironment of HPV-positive and HPV-negative oropharyngeal squamous cell carcinoma: a multiparametric quantitative and spatial analysis unveils a rationale to target treatment-naïve tumors with immune checkpoint inhibitors. J Exp Clin Cancer Res. 2022;41(1):279. https://doi.org/10.1186/s13046-022-02481-4

12. Jiang Y, Zhang S, Tang L, Li R, Zhai J, Luo S, et al. Single-cell RNA sequencing reveals TCR+ macrophages in HPV-related head and neck squamous cell carcinoma. Front Immunol. 2022;13:1030222. https://doi.org/10.3389/fimmu.2022.1030222

13. Lee H, Park S, Yun JH, Seo C, Ahn JM, Cha HY, et al. Deciphering head and neck cancer microenvironment: single-cell and spatial transcriptomics reveals human papillomavirus-associated differences. J Med Virol. 2024;96(1):e29386. https://doi.org/10.1002/jmv.29386

14. Markovits E, Klymyshyn D, Froumine R, Zong H, Mints M, Mahadevan S, et al. Spatial profiling of HPV-stratified head and neck squamous cell carcinoma reveals distinct immune niches and microenvironmental architectures. J Transl Med. 2025;23(1):1304. https://doi.org/10.1186/s12967-025-07280-x

15. Liu C, Wu K, Li C, Zhang Z, Zhai P, Guo H, et al. SPP1+ macrophages promote head and neck squamous cell carcinoma progression by secreting TNF-α and IL-1β. J Exp Clin Cancer Res. 2024;43(1):332. https://doi.org/10.1186/s13046-024-03255-w

16. Wu J, Pang X, Yang X, Zhang M, Chen B, Fan H, et al. M1 macrophages induce PD-L1hi cell-led collective invasion in HPV-positive head and neck squamous cell carcinoma via TNF-α/CDK4/UPS14. J Immunother Cancer. 2023;11(12):e007670. https://doi.org/10.1136/jitc-2023-007670

EARLY ACCESS

17. Zhang N, Xu Z, Tian G, Deng W, Xu J, Huang C, et al. Distinct single-cell cellular states and ecosystems linked to HPV status distinguish therapeutic vulnerability of head and neck squamous cell carcinoma. Commun Biol. 2026;9(1):954. https://doi.org/10.1038/s42003-026-10213-z

18. Mints M, Sample RA, Parikh AS, Zaretsky JM, Qi Z, Law T, et al. Single-cell analysis highlights the significance of malignant cell IFN/MHC-II for immunotherapy response in head and neck squamous cell carcinoma. Cell Rep Med. 2026;7(4):102715. https://doi.org/10.1016/j.xcrm.2026.102715

19. Simkin D, Barrett TF, Zhang L, Moore MJ, Greenwald AC, Galili N, et al. Spatial analysis of head and neck cancer identifies two ecosystems with distinct modes of epithelial-to-mesenchymal transition. Nat Genet. 2026;58(9):2240–53. https://doi.org/10.1038/s41588-026-02723-7

20. Stuart T, Butler A, Hoffman P, Hafemeister C, Papalexi E, Mauck WM 3rd, et al. Comprehensive integration of single-cell data. Cell. 2019;177(7):1888–902.e21. https://doi.org/10.1016/j.cell.2019.05.031

21. Hao Y, Stuart T, Kowalski MH, Choudhary S, Hoffman P, Hartman A, et al. Dictionary learning for integrative, multimodal and scalable single-cell analysis. Nat Biotechnol. 2024;42(2):293–304. https://doi.org/10.1038/s41587-023-01767-y

22. Korsunsky I, Millard N, Fan J, Slowikowski K, Zhang F, Wei K, et al. Fast, sensitive and accurate integration of single-cell data with Harmony. Nat Methods. 2019;16(12):1289–96. https://doi.org/10.1038/s41592-019-0619-0

23. Trapnell C, Cacchiarelli D, Grimsby J, Pokharel P, Li S, Morse M, et al. The dynamics and regulators of cell fate decisions are revealed by pseudotemporal ordering of single cells. Nat Biotechnol. 2014;32(4):381–6. https://doi.org/10.1038/nbt.2859

24. Cao J, Spielmann M, Qiu X, Huang X, Ibrahim DM, Hill AJ, et al. The single-cell transcriptional landscape of mammalian organogenesis. Nature. 2019;566(7745):496–502. https://doi.org/10.1038/s41586-019-0969-x

EARLY ACCESS

25. Kang M, Gulati GS, Brown EL, Qi Z, Avagyan S, Armenteros JJA, et al. Improved reconstruction of single-cell developmental potential with CytoTRACE 2. Nat Methods. 2025;22(11):2258–63. https://doi.org/10.1038/s41592-025-02857-2

26. Subramanian A, Tamayo P, Mootha VK, Mukherjee S, Ebert BL, Gillette MA, et al. Gene set enrichment analysis: a knowledge-based approach for interpreting genome-wide expression profiles. Proc Natl Acad Sci U S A. 2005;102(43):15545–50. https://doi.org/10.1073/pnas.0506580102

27. Liberzon A, Birger C, Thorvaldsdóttir H, Ghandi M, Mesirov JP, Tamayo P. The Molecular Signatures Database (MSigDB) hallmark gene set collection. Cell Syst. 2015;1(6):417–25. https://doi.org/10.1016/j.cels.2015.12.004

28. Jin S, Guerrero-Juarez CF, Zhang L, Chang I, Ramos R, Kuan CH, et al. Inference and analysis of cell-cell communication using CellChat. Nat Commun. 2021;12(1):1088. https://doi.org/10.1038/s41467-021-21246-9

29. Aibar S, González-Blas CB, Moerman T, Huynh-Thu VA, Imrichova H, Hulselmans G, et al. SCENIC: single-cell regulatory network inference and clustering. Nat Methods. 2017;14(11):1083–6. https://doi.org/10.1038/nmeth.4463

30. Kumar N, Mishra B, Athar M, Mukhtar S. Inference of gene regulatory network from single-cell transcriptomic data using pySCENIC. Methods Mol Biol. 2021;2328:171–82. https://doi.org/10.1007/978-1-0716-1534-8_10

31. Osorio D, Zhong Y, Li G, Xu Q, Yang Y, Tian Y, et al. scTenifoldKnk: an efficient virtual knockout tool for gene function predictions via single-cell gene regulatory network perturbation. Patterns (N Y). 2022;3(3):100434. https://doi.org/10.1016/j.patter.2022.100434

32. Wu T, Hu E, Xu S, Chen M, Guo P, Dai Z, et al. clusterProfiler 4.0: a universal enrichment tool for interpreting omics data. Innovation (Camb). 2021;2(3):100141. https://doi.org/10.1016/j.xinn.2021.100141

33. Hsu DS, Wang HJ, Tai SK, Chou CH, Hsieh CH, Chiu PH, et al. Acetylation of Snail modulates the cytokinome of cancer cells to enhance the recruitment of macrophages. Cancer Cell. 2014;26(4):534–48. https://doi.org/10.1016/j.ccell.2014.09.002

EARLY ACCESS

34. Bao Z, Zeng W, Zhang D, Wang L, Deng X, Lai J, et al. SNAIL induces EMT and lung metastasis of tumours secreting CXCL2 to promote the invasion of M2-type immunosuppressed macrophages in colorectal cancer. Int J Biol Sci. 2022;18(7):2867–81. https://doi.org/10.7150/ijbs.66854

35. Bill R, Wirapati P, Messemaker M, Roh W, Zitti B, Duval F, et al. CXCL9:SPP1 macrophage polarity identifies a network of cellular programs that control human cancers. Science. 2023;381(6657):515–24. https://doi.org/10.1126/science.ade2292

36. Wu Z, Cheng C, Li Z, Ren M, Cao H, Huang W, et al. Comprehensive tumour-immune profiling reveals TREM2+ tumour-associated macrophages facilitating lymph node metastasis in head and neck squamous cell carcinoma. Clin Transl Med. 2026;16(2):e70604. https://doi.org/10.1002/ctm2.70604

EARLY ACCESS

FIGURES WITH LEGENDS

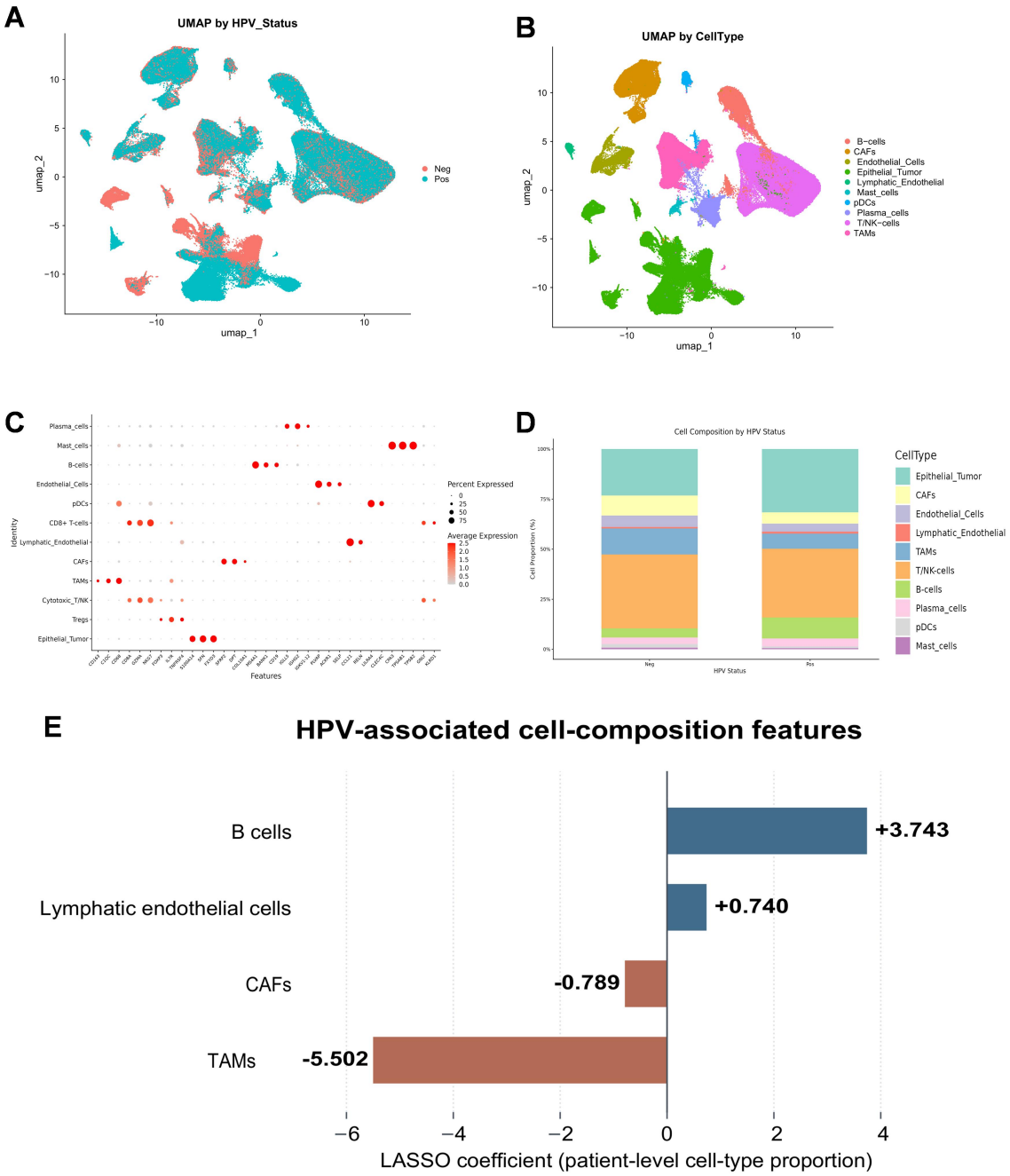


Figure 1. Cellular landscape and HPV-associated cell composition in HNSCC. (A) UMAP of the integrated dataset of 229,196 single cells from 59 patients, colored by HPV status. **(B)** UMAP colored by the 10 major cell lineages. **(C)** Expression of canonical markers supporting lineage annotation. **(D)** Pooled cell-type proportions by HPV status; these are descriptive cell-level summaries. **(E)** Patient-level LASSO regression coefficients for HPV-status classification. **Abbreviations:** CAF, cancer-associated fibroblast; HNSCC, head and neck squamous cell carcinoma; HPV, human papillomavirus; LASSO, least absolute shrinkage and selection operator; Neg, HPV-

negative; NK, natural killer; pDC, plasmacytoid dendritic cell; Pos, HPV-positive; TAM, tumor-associated macrophage; Treg, regulatory T cell; UMAP, uniform manifold approximation and projection.

EARLY ACCESS

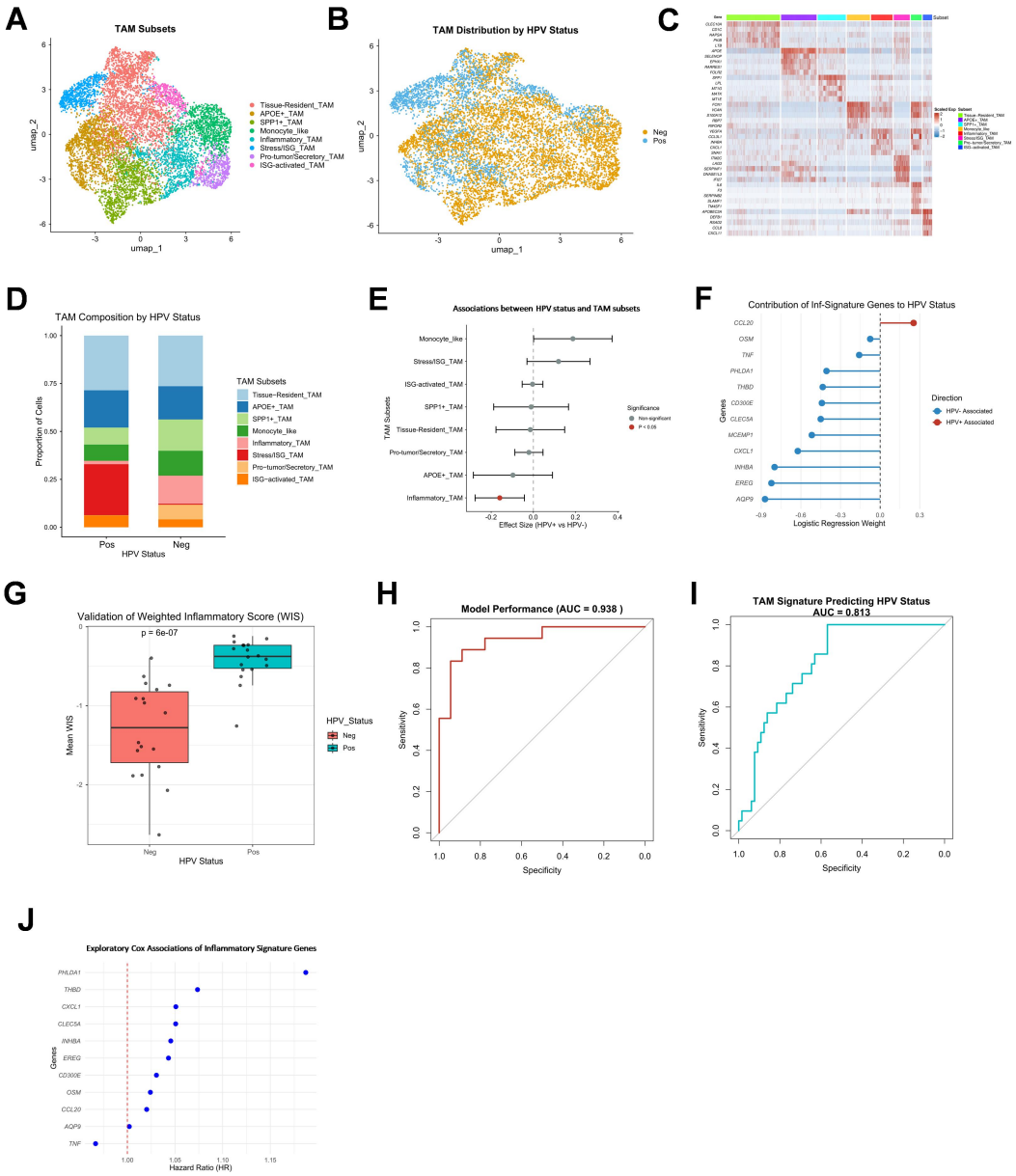


Figure 2. TAM-state heterogeneity and the 12-gene WIS. (A) UMAP of eight TAM states. **(B)** Distribution of TAMs by HPV status. **(C)** State-specific marker expression. **(D)** Pooled TAM-state composition by HPV status, showing descriptive cell-level proportions. **(E)** HPV-positive-minus-HPV-negative TAM-state effect estimates from an exploratory model, with horizontal uncertainty intervals and colors indicating nominal statistical significance. Final BH-adjusted patient-level comparisons and separate regression analyses are reported in Table S2. **(F)** Regression coefficients for the 12-gene WIS. **(G)** Patient-level WIS distributions by HPV status among 36 validation patients (GSE181919, *n* = 20; GSE182227, *n* = 16). **(H)** Fixed-weight WIS discrimination in the pooled external validation sample (AUC 0.938; 95% CI 0.863–1.000; *n* = 36). **(I)** A separately fitted TCGA-internal ssGSEA

classifier using the same 12 genes (AUC 0.813); this is distinct from external validation of the fixed WIS. **(J)** Exploratory TCGA gene-level HR estimates; these findings are not adjusted for multiple comparisons. **Abbreviations:** AUC, area under the receiver operating characteristic curve; BH, Benjamini–Hochberg; CI, confidence interval; HPV, human papillomavirus; HR, hazard ratio; ISG, interferon-stimulated gene; Neg, HPV-negative; Pos, HPV-positive; ssGSEA, single-sample gene set enrichment analysis; TAM, tumor-associated macrophage; TCGA, The Cancer Genome Atlas; UMAP, uniform manifold approximation and projection; WIS, weighted inflammatory score.

EARLY ACCESS

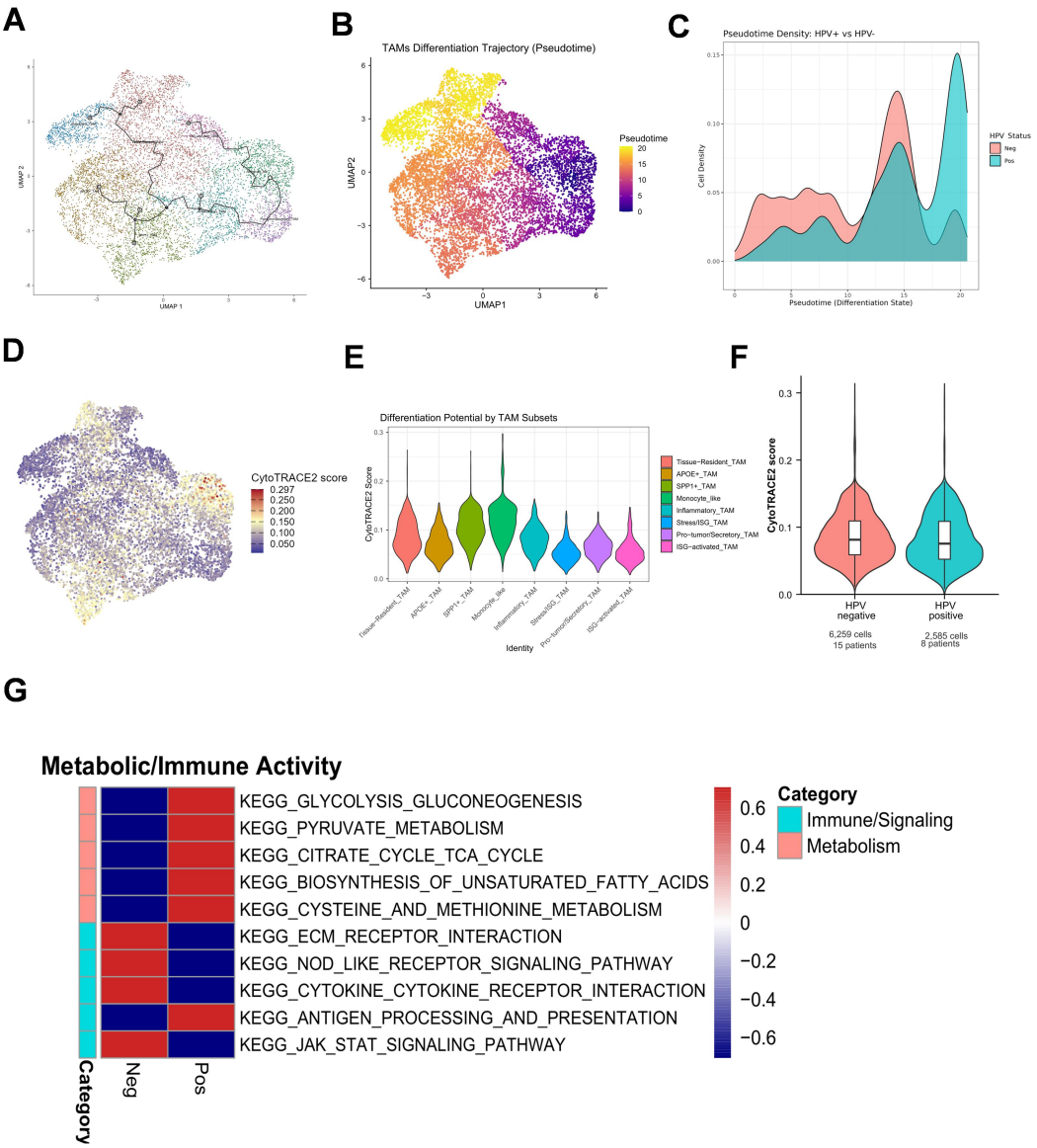


Figure 3. TAM trajectories, inferred developmental potential, and metabolic and immune programs. **(A)** Monocle3 trajectory over the TAM embedding. **(B)** Monocle3-inferred pseudotime. **(C)** Descriptive pseudotime density distributions in HPV-negative and HPV-positive TAMs, without cell-level significance testing. **(D)** UMAP of 8,922 TAMs colored by continuous CytoTRACE2 scores (approximately 0.008–0.297). **(E)** CytoTRACE2 score distributions across the eight TAM states. **(F)** Cell-level CytoTRACE2 score distributions in GSE234933 TAMs by HPV status. Violin plots show score distributions; inset boxplots indicate the median and interquartile range. **(G)** Selected metabolic and immune pathway activity scores in HPV-negative (Neg) and HPV-positive (Pos) cells. Pathway categories are annotated on the left; red and blue indicate relatively higher and lower displayed activity, respectively. Trajectory and developmental-potential patterns are computationally

inferred. **Abbreviations:** ECM, extracellular matrix; HPV, human papillomavirus; ISG, interferon-stimulated gene; KEGG, Kyoto Encyclopedia of Genes and Genomes; Neg, HPV-negative; Pos, HPV-positive; TAM, tumor-associated macrophage; TCA, tricarboxylic acid; UMAP, uniform manifold approximation and projection.

EARLY ACCESS

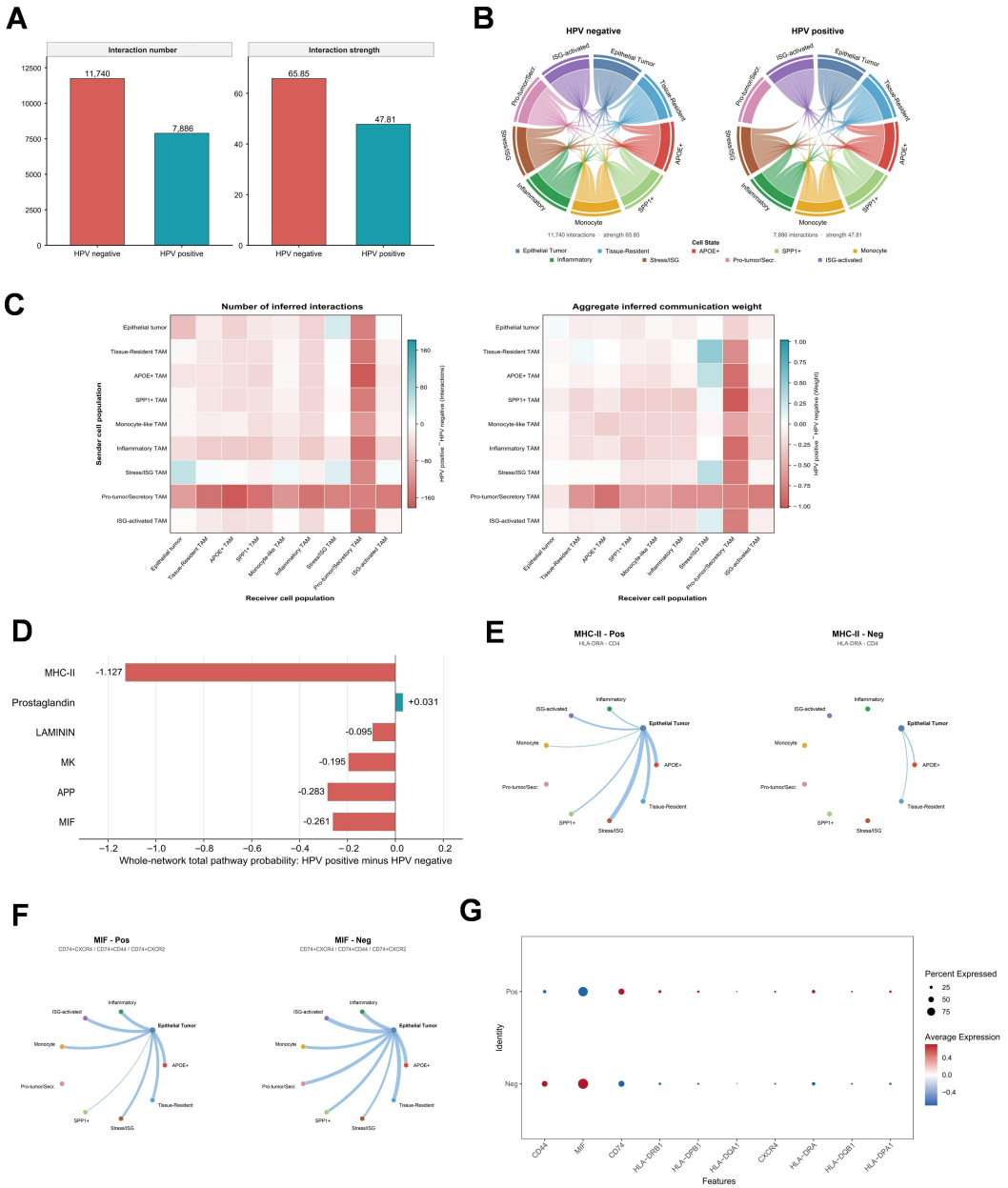


Figure 4. HPV-associated differences in inferred epithelial–TAM communication. **(A)** Numbers and aggregate weights of CellChat-inferred interactions in HPV-negative and HPV-positive GSE234933 tumors. **(B)** Inferred networks among epithelial tumor cells and eight TAM states. Arrows indicate source-to-recipient direction, and edge widths represent inferred interaction counts. **(C)** Source–recipient heatmaps showing HPV-positive-minus-HPV-negative differences in inferred interaction numbers and aggregate weights. **(D)** Corresponding differences in selected whole-network pathway probabilities, including MHC-II and MIF. **(E)** Candidate epithelial-source MHC-II connections: the database-annotated HLA-DRA–CD4 entry connects to seven TAM recipient states in HPV-positive tumors and two in HPV-negative tumors. **(F)** Epithelial-source MIF-associated connections involving MIF–

(CD74+CD44), MIF–(CD74+CXCR4), and MIF–(CD74+CXCR2). **(G)** Expression of selected MHC-II- and MIF-associated genes in epithelial tumor cells. Dot size indicates the percentage of cells expressing each gene, and color indicates average expression. Network connections are computationally inferred; detailed source–target records are provided in Table S6. **Abbreviations:** HPV, human papillomavirus; ISG, interferon-stimulated gene; MHC-II, major histocompatibility complex class II; Neg, HPV-negative; Pos, HPV-positive; TAM, tumor-associated macrophage.

EARLY ACCESS

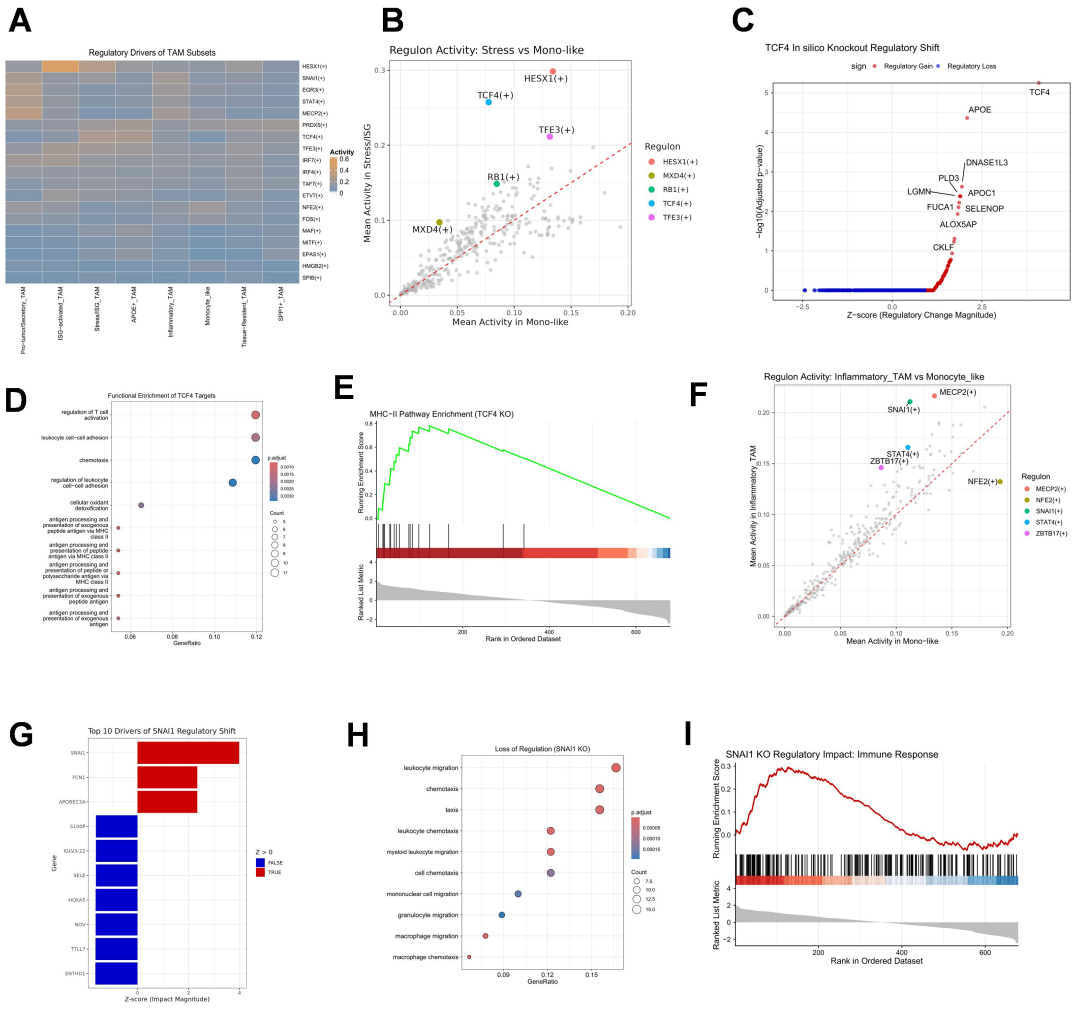


Figure 5. Candidate SNAI1- and TCF4-associated regulatory programs in TAMs. **(A)** pySCENIC regulon activity across eight TAM states. **(B)** Stress/ISG-versus-Monocyte-like regulon activities, highlighting TCF4, HESX1, and TFE3. **(C)** Predicted regulatory shifts following virtual TCF4 knockout with scTenifoldKnk. **(D)** Functional enrichment of TCF4-associated regulatory changes. **(E)** MHC-II-related gene-set enrichment following virtual TCF4 perturbation. **(F)** Inflammatory-versus-Monocyte-like regulon activities, highlighting SNAI1 and MECP2. **(G)** Predicted regulatory shifts following virtual SNAI1 knockout. **(H)** Migration- and chemotaxis-associated enrichment of SNAI1-affected network genes. **(I)** Immune-response gene-set enrichment following virtual SNAI1 perturbation. Virtual knockout identifies predicted network responses rather than laboratory knockout outcomes. **Abbreviations:** ISG, interferon-stimulated gene; KO, knockout; MHC-II, major histocompatibility complex class II; pySCENIC, Python implementation of single-cell regulatory network inference and clustering; TAM, tumor-associated macrophage.

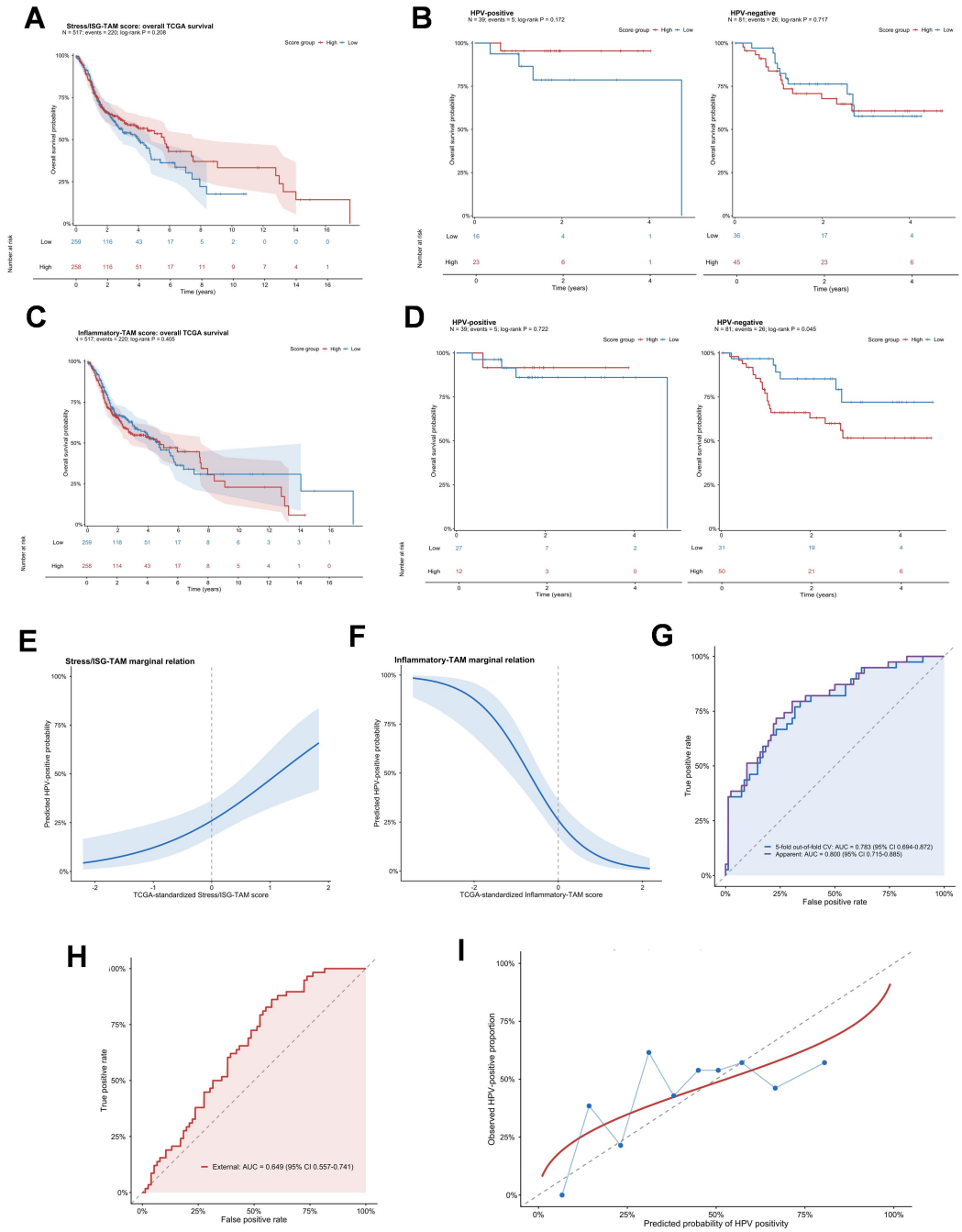


Figure 6. TAM-state signature associations and HPV-status discrimination with TRS. (A) Kaplan–Meier overall survival by high versus low Stress/ISG-TAM signature in the full TCGA survival cohort (*n* = 517). **(B)** Stress/ISG-TAM survival curves by HPV status, with numbers at risk. **(C)** Overall survival by Inflammatory-TAM signature in the full cohort. **(D)** Inflammatory-TAM survival curves by HPV status, with numbers at risk. High/low groups use the median score of the full survival cohort. Nominal log-rank *p* values are shown in the plots; multiplicity-adjusted results are reported in the text and Table S5. **(E,F)** Model-based marginal predicted probabilities of HPV positivity across standardized Stress/ISG-TAM and

Inflammatory-TAM scores, respectively, with the other predictor held fixed. **(G)** Apparent and fivefold patient-level out-of-fold ROC curves in TCGA (n = 121). **(H)** External ROC curve for the fixed TRS model in GSE40774 (n = 134). **(I)** External calibration in GSE40774: observed HPV-positive proportions (blue), ideal calibration (dashed line), and the fitted logistic recalibration curve (red). **Abbreviations:** AUC, area under the receiver operating characteristic curve; CI, confidence interval; CV, cross-validation; HPV, human papillomavirus; ISG, interferon-stimulated gene; ROC, receiver operating characteristic; TAM, tumor-associated macrophage; TCGA, The Cancer Genome Atlas; TRS, TAM-related score.

EARLY ACCESS

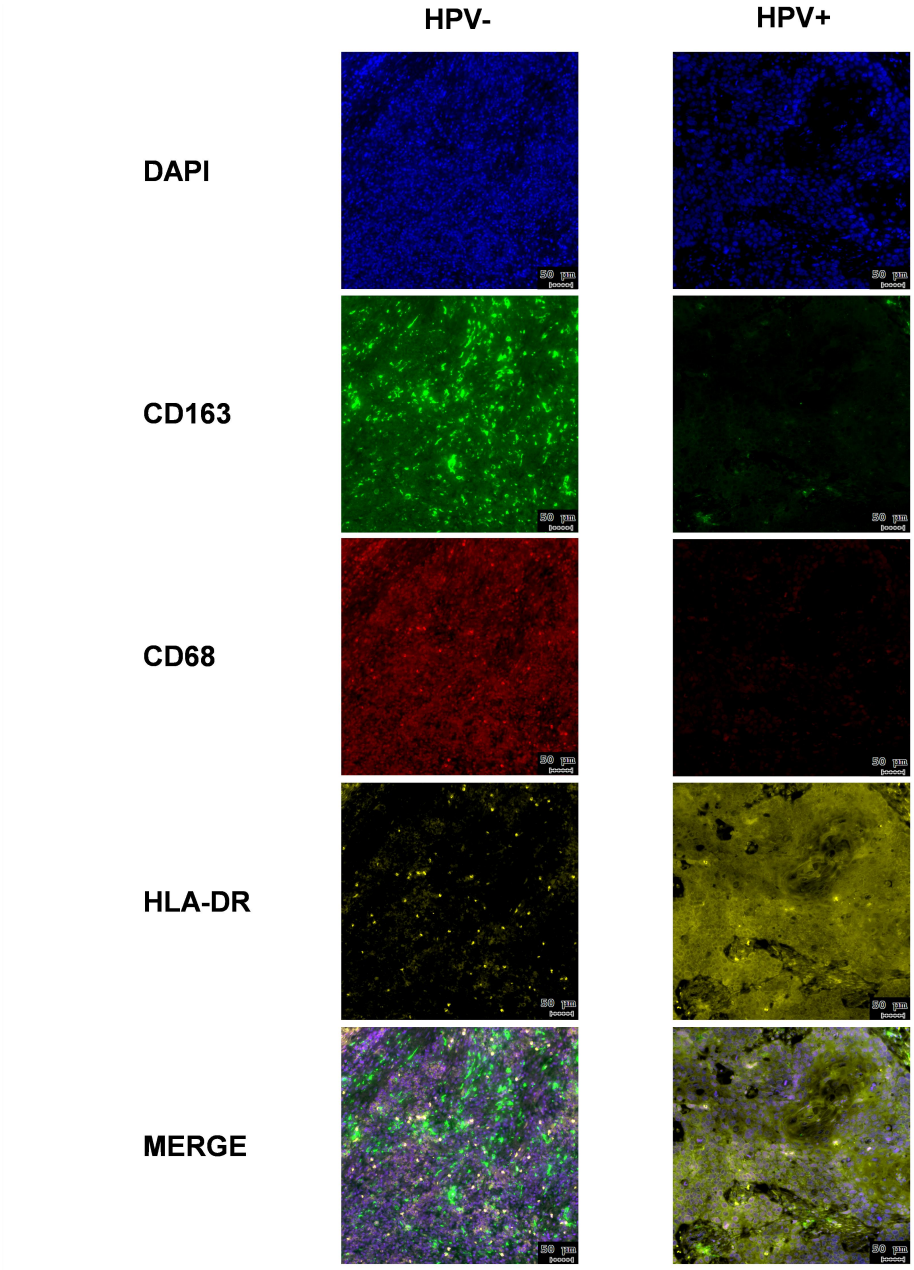


Figure 7. Representative multiplex immunofluorescence in HPV-negative and HPV-positive HNSCC. Tissue sections were examined from 10 patients (five HPV-positive and five HPV-negative). One representative field from each HPV group is shown. Separate channels and merged images display DAPI (blue), CD163 (green), CD68 (red), and HLA-DR (yellow). In these selected fields, the HPV-negative example shows more conspicuous CD68/CD163-associated fluorescence, whereas the HPV-positive example shows more conspicuous HLA-DR-associated fluorescence. Scale bars, 50 μm. These images provide illustrative tissue-level observations; no patient-level quantitative group comparison is inferred from the representative fields.

Abbreviations: DAPI, 4′,6-diamidino-2-phenylindole; HNSCC, head and neck squamous cell carcinoma; HPV, human papillomavirus.

EARLY ACCESS

SUPPLEMENTAL DATA

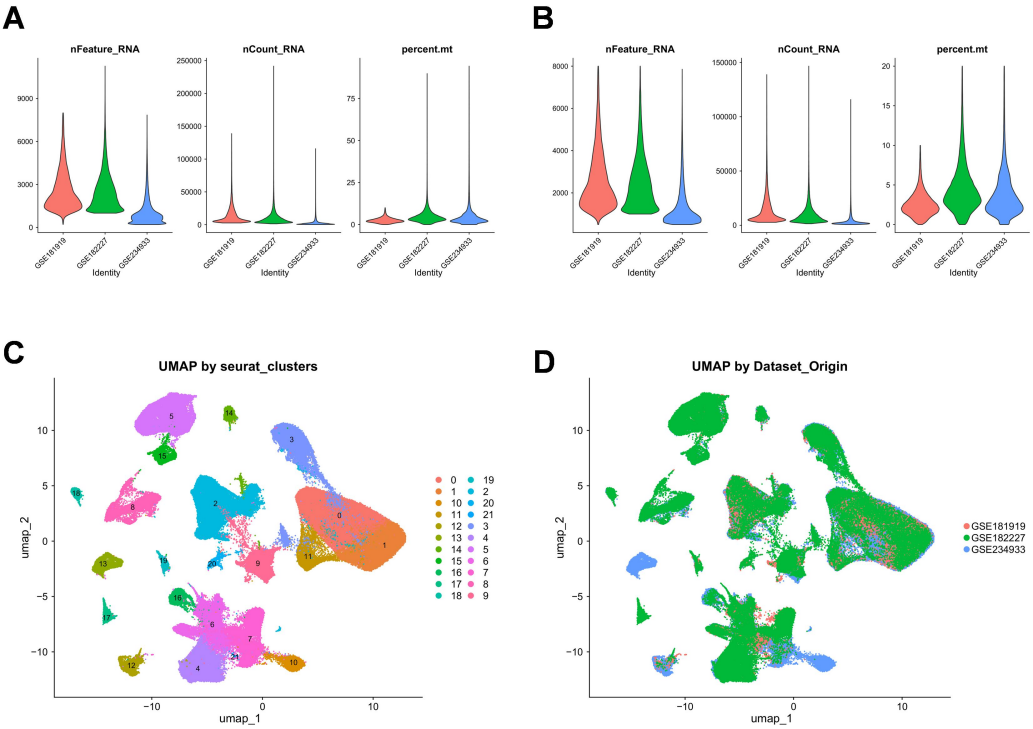


Figure S1. Single-cell quality control and the integrated HNSCC cell landscape. **(A)** Distributions of detected genes (nFeature_RNA), total RNA counts (nCount_RNA), and mitochondrial transcript percentage (percent.mt) across GSE181919, GSE182227, and GSE234933 before quality-control filtering. **(B)** Distributions of the same metrics after filtering. **(C)** UMAP of the integrated cell dataset colored by Seurat cluster identifier. **(D)** The same integrated UMAP colored by dataset of origin. Panels C and D show the distribution of integrated cells and do not constitute a direct before-versus-after batch-correction comparison. **Abbreviations:** HNSCC, head and neck squamous cell carcinoma; UMAP, uniform manifold approximation and projection.

Supplemental code and Tables S1-S6 are available at the following link: https://www.bjbms.org/ojs/index.php/bjbms/article/view/14972

EARLY ACCESS